JOURNAL OF AIRCRAFT
Vol. 48, No. 4, July–August 2011

Gust-Response Analysis of Free Elastic Aircraft in the Transonic Flight Regime

Daniella E. Raveh*
Technion–Israel Institute of Technology, Haifa 32000, Israel

DOI: 10.2514/1.C031224

The study presents a methodology for introducing computational fluid dynamics to gust-response analysis in a computationally efficient manner. Two approaches for computational-fluid-dynamics-based gust-response analysis of free elastic aircraft are presented. The direct approach involves full aeroelastic simulation within the computational fluid dynamics run. The hybrid approach involves computing rigid sharp-edge gust responses in a computational fluid dynamics run, computing the gust input forces due to arbitrary gust profiles via convolution, and applying a linear aeroelastic feedback loop to compute the aeroelastic gust responses. The latter is highly computationally efficient, as only one relatively short computational fluid dynamics run is required for the computation of the sharp-edge gust response, after which responses to arbitrary gust profiles can be computed in seconds. The former is more elaborate and time-consuming and can be used in cases of critical responses. The use of the two methods is demonstrated on a transport aircraft, flying trimmed at Mach 0.85, 10,000 ft, that passes through one-minus-cosine shaped gusts, as required by the Federal Aviation Regulations.

Nomenclature

b	=	half-chord length, m
$\{GF_A\}$	=	generalized aerodynamic forces, Nm
$\{GF_G\}$	=	gust generalized aerodynamic forces, Nm
$[GK]$	=	generalized stiffness matrix, Nm
$[GM]$	=	generalized mass matrix, kg m^2
L_G	=	gust gradient length, m
$[Q]$	=	aerodynamic force coefficient matrix
t	=	time, s
V	=	flight speed, m/s
w_G	=	gust-induced vertical velocity, m/s
$\bar{w}_G$	=	gust velocity amplitude, m/s
x	=	coordinate along the aircraft's longitudinal axis, m
$\{\xi\}$	=	generalized displacements
$[\phi]$	=	modal matrix, m
$\{\Psi\}$	=	aerodynamic transfer function, N

I. Introduction

PRODUCTION methods for dynamic gust analysis typically rely on linear, frequency-domain, panel aerodynamic methods that are used in conjunction with the frequency-domain formulation of the aeroelastic equations of motion [1–4]. In low-speed flight near stall or in flight in the transonic regime, the aerodynamic forces are no longer linearly dependent on the flight angle of attack and thus cannot be accurately predicted by linear aerodynamic methods. Gust-response analysis has to be supported with some nonlinear aerodynamic model [5]. Aerodynamic nonlinearities associated with gust response have significant impact on both aircraft handling qualities and structural design. In the extremely low flight speeds, gust vertical velocities may induce angles of attacks beyond stall; in the transonic speeds, the aerodynamic nonlinearity implies that the loads due to gust may be different from those predicted by linear aerodynamics. Both of these gust-related nonlinear phenomena have to be accounted for in the design of a new airplane configuration. The need to introduce nonlinear aerodynamics into aircraft gust-response analysis and design is critical when new technologies and configurations are designed, such as the high-altitude, long-endurance (HALE) configuration. A HALE wing is typically of very high aspect ratio, extremely elastic, and therefore highly susceptible to large deformations and dynamic elastic responses when subjected to atmospheric turbulence.

A recent study [6] presented a method of using computational fluid dynamics (CFD) tools for dynamic gust-response analysis, both via direct numerical simulation and via reduced-order modeling (ROM) of the aerodynamic rigid gust forces. The advantages of using CFD tools for gust-response analysis are fourfold:

1) CFD analysis offers various levels of accurate aerodynamic modeling that are adequate for various flight regimes.

2) CFD models are unsteady time-domain models and are therefore suitable for dynamic response analysis.

3) CFD methods accurately predict the development of gust forces, as they correctly account for the propagation of the gust interference throughout the flowfield in the speed of sound.

4) Navier–Stokes turbulent CFD models are capable of predicting the aerodynamic load decrease associated with flight at high angles of attack, close to stall.

Therefore, when used for gust analysis, such methods can better predict the gust loads at all flight speeds and allow for high-fidelity aeroelastic design.

In recent years, several studies have addressed CFD-based gust-response analysis. Zaide and Raveh [7] simulated time histories of the aerodynamic response of two-dimensional airfoils to arbitrary gust inputs and validated the gust responses by comparison to the closed-form Kussner functions in the subsonic and transonic flow regimes. Gust velocity inputs were introduced into the EZNSS [8] (Elastic Zonal Navier–Stokes Simulation) CFD code using the field-velocity method, proposed by Parameswaran and Baeder [9] and practiced by Singh and Baeder [10,11]. Yang and Obayashi [12] presented CFD gust simulation of a complete aircraft configuration to one-minus-cosine gust profile, using two rigid-body degrees of freedom of pitch and plunge, with and without elastic effects.

Raveh [13] presented CFD simulation and reduced-order modeling of a clamped rigid wing in response to traveling-gust excitations. Four ROMs were evaluated: a convolution model that is based on CFD-computed sharp-edge gust response, two parametric autoregressive moving-average and state-space models and a frequency-response model. Models of the lift coefficient, root

Presented as Paper 2010-3050 at the Structures, Structural Dynamics, and Materials Conference, Orlando, FL, 12–15 April 2010; received 2 September 2010; revision received 14 March 2011; accepted for publication 15 March 2011.

*Senior Lecturer, Faculty of Aerospace Engineering. Senior Member AIAA.

bending moment, and gust generalized aerodynamic forces were developed and used to compute responses to discrete and continuous gust excitations. The purpose of that study was to examine the suitability (that is, the accuracy, the computational cost, and the ease of application) of various ROMs for replacing a full CFD simulation. Validation was achieved through comparison of the responses from these models to those computed directly in CFD simulations. Convolution models were found to be very appropriate for gust-response applications; thus, they were applied and examined in a study of gust analysis of a free elastic aircraft configuration [6]. Raveh [6] presented two CFD-based gust analysis methods: 1) a complete CFD aeroelastic simulation, including elastic and rigid-body motions and 2) a hybrid aeroelastic simulation in which the rigid gust forces are CFD-based (provided by convolution of the gust velocity profile with CFD-based sharp-edge gust responses), and the aeroelastic feedback is based on linear aerodynamics (state-space model). The methodology was demonstrated using a generic transport model that was excited by one-minus-cosine gust profiles. Comparison with gust responses computed by ZAERO [4] linear panel code served for verification of the proposed methods and also to indicate similarities and differences between gust responses computed by a linear and a nonlinear aerodynamic method.

The current study uses the direct- and hybrid-simulation methods and the models of [6] to study dynamic gust response of a free elastic aircraft in the transonic flight regime, in flight conditions at which the loads due to gust deviate from linear. The study investigates the differences in gust loads computed using linear and nonlinear aerodynamic theories. Also, the hybrid ROM method of this study is based on the use of convolution for prediction of rigid gust forces. The study examines the adequacy of the use of convolution in the presence of aerodynamic nonlinearities.

II. Methodology

The aeroelastic equation of motion for an aircraft in response to atmospheric gust excitation, in generalized coordinates, neglecting damping, is stated as

$$[GM]\{\ddot{\xi}\} + [GK]\{\xi\} - \{GF_A(t)\} = \{GF_G(t)\} \tag{1}$$

where $\{\xi\}$ is the vector of generalized displacements (including rigid-body and elastic displacements), and $[GM]$ and $[GK]$ are the generalized mass and stiffness matrices of the structure. $\{GF_A(t)\}$ and $\{GF_G(t)\}$ are the vectors of generalized aerodynamic forces (GAFs) and gust generalized aerodynamic forces (GGAFs), respectively. The GAFs are dependent on the structural deformations, their time histories, and the time histories of the generalized aerodynamic forces themselves. The GGAFs are due to discrete traveling-gust excitation. They are dependent on the velocity profile of the gust input and on the histories of the gust forces. It is important to note that the gust forces are independent of the structural deformations. This implies that the GGAFs on the right-hand side of Eq. (1) can be computed separately, ahead of the simulation of Eq. (1), and presented as a fixed time-dependent input vector when simulating Eq. (1). This is unlike the GAFs that must be reevaluated in every step of the simulation of Eq. (1). When considering CFD tools for gust aeroelastic analysis, this may present significant computational savings if CFD analysis is only used to compute the GGAFs.

In flight conditions in which the elastic response is expected to be linear, CFD analysis can be used only for the computation of the GGAFs, on the right-hand side of Eq. (1), while the elastic analysis can be carried out using traditional linear aeroelastic feedback. In flight conditions in which the aeroelastic response is expected to be nonlinear (that is, the aerodynamic forces due to elastic deformations depend nonlinearly on the deformations), Eq. (1) can be integrated fully in a CFD simulation, accounting for all nonlinearities. An in-between option for mildly nonlinear aeroelastic responses could be to use CFD-based ROMs for the aeroelastic response of the left-hand side of Eq. (1), as proposed in [14].

The current study presents two methods for CFD-based gust analysis. In the first method, a CFD-based convolution ROM for the GGAFs is computed and used in the aeroelastic simulation of Eq. (1), in which the GAFs are based on traditional, linear, state-space formulation. The second method is a full simulation of the aeroelastic equation (1) in an elastic CFD analysis. Generalized forces and displacements computed by the two methods are compared. These responses are also compared with a linear gust-response simulation performed by the commercial aeroelastic software ZAERO [4], in order to compare loads computed based on linear and nonlinear theories.

A. Gust Convolution Reduced-Order Model

We consider a discrete gust with an arbitrary velocity distribution profile f in the flow direction and a uniform velocity distribution in the spanwise direction. The latter can be expanded straightforwardly to account for nonuniform velocity distribution for cases of high-span wings. The gust travels over the aircraft at the constant flight speed V, starting at the aircraft's nose at time zero. This gust induces at time t, at location x on the aircraft (x is measured in the flow direction, with origin at the aircraft's nose), and a vertical velocity of

$$w_G(t) = \begin{cases} \bar{w}_G f(t - x/V) & t > x/V \\ 0 & t < x/V \end{cases} \tag{2}$$

where $\bar{w}_G$ is the gust velocity amplitude. A sharp-edge gust input profile is defined as a traveling gust of constant vertical velocity, as

$$w_{\mathrm{SEG}}(t) = \begin{cases} \bar{w}_{\mathrm{SEG}} & t > x/V \\ 0 & t < x/V \end{cases} \tag{3}$$

$\{GF_{\mathrm{SEG}}(t)\}$, the GGAFs due to a sharp-edge gust excitation, are simulated in a CFD run. The gust velocities are introduced to the CFD computation, at each time-iteration, by prescribing the gust vertical velocity to all grid points with flow-direction coordinate x of $x \le tV$. These gust vertical velocities are assigned to the CFD grid time metrics, without actually moving the grid, following the field-velocity method [7,9–11]. The generalized forces due to sharp-edge gust are computed at each time step of the CFD analysis according to

$$\{GF_{\mathrm{SEG}}(t)\} = [\phi]^T\{\Psi(t)\} \tag{4}$$

where $\{\Psi(t)\}$ is the aerodynamic transfer function; $\{\Psi(t)\}$ contains the time-dependent aerodynamic forces, computed at the CFD surface grid points, in response to a sharp-edge gust excitation of $\bar{w}_{\mathrm{SEG}}$ amplitude; and $[\phi]$ is the modal matrix, in which each column represents an elastic mode shape. The mode shapes, which are typically computed by structural finite elements at the finite element model nodes, are mapped to the CFD surface grids, at which the gust forces are computed, in order to perform the matrix multiplication of Eq. (4). It is noted that the modes of Eq. (4) may be rigid-body or elastic modes, or any other mode shapes. For example, when $\{\phi\}$ is a unit-displacement heave mode, the generalized gust force of Eq. (4) is the time-dependent total lift due to the sharp-edge gust. Similarly, the root bending moment due to the sharp-edge gust can be computed by using a mode that holds the moment arms from each CFD grid to the wing root (a load mode).

Using the CFD-simulated sharp-edge GGAFs, the time history of forces due to arbitrary gust input [the right-hand side of Eq. (1)], can be computed via convolution, as

$$\{GF_G(t)\} = \int_0^t \dot{w}_G(\tau) GF_{\mathrm{SEG}}(t - \tau)\,\mathrm{d}\tau \tag{5}$$

where $\dot{w}_G(t)$ is the time derivative of the gust input velocity. The use of convolution according to Eq. (5) assumes that the superposition of gust loads is valid; i.e., the gust-induced velocities are not large enough to cause stall or any other nonlinear aerodynamic effect.

In the current study, gust inputs considered are one-minus-cosine gusts, required by the Federal Aviation Administration for aircraft certification. A one-minus-cosine gust input is defined as

$$w_G(t) = \begin{cases} \frac{1}{2}\bar{w}_G\left(1 - \cos\frac{2\pi(t-x/V)}{L_G/V}\right) & tV - L_G < x < tV \\ 0 & \text{otherwise} \end{cases} \quad (6)$$

where L_G is the gust length (in length units).

The GGAFs computed by Eq. (5) can be introduced to the right-hand side of the aeroelastic equation of motion (1) to form the aeroelastic gust-response equation:

$$[GM]\{\ddot{\xi}\} + [GK]\{\xi\} - \{GF_A(t)\} = \int_0^t \dot{w}_G(\tau) GF_{\text{SEG}}(t-\tau)\,\mathrm{d}\tau \quad (7)$$

Equation (7) can be solved for ξ using numerical integration schemes. Since the gust excitation force on the right-hand side is independent of the displacements ξ, it can be computed in advance, ahead of the simulation of Eq. (7). Also, it is independent of the model used for the estimation of the aerodynamic forces due to elastic deformations on the left-hand side. In the following section the well-known state-space formulation of the aeroelastic equation, with the minimum-state aerodynamic approximation [15], is used for the left-hand-side aeroelastic forces. The formulation is repeated below.

B. State-Space Formulation of the Aeroelastic System

The aeroelastic equation of motion in response to gust excitation [Eq. (1)] can be written in state-space form as

$$\begin{aligned} \dot{x}_S(t) &= \bar{A}_S x_S(t) + \bar{B}_S GF_A(t) + \bar{B}_{SG} GF_G(t) \\ \xi(t) &= \bar{C}_S x_S(t) + \bar{D}_S GF_A(t) + \bar{D}_{SG} GF_G(t) \end{aligned} \quad (8)$$

where x_S is the state vector,

$$x_S(t) = \begin{Bmatrix} \xi \\ \dot{\xi} \end{Bmatrix} \quad (9)$$

and the coefficient matrices are defined as follows:

$$\bar{A}_S = \begin{bmatrix} 0 & 1 \\ -GM^{-1}GK & 0 \end{bmatrix} \quad \bar{B}_S = \begin{bmatrix} 0 \\ GM^{-1} \end{bmatrix} \quad \bar{B}_{SG} = \begin{bmatrix} 0 \\ GM^{-1} \end{bmatrix}$$
$$\bar{C}_S = [I \quad 0] \qquad \bar{D}_S = [0] \qquad \bar{D}_{SG} = [0] \quad (10)$$

The aerodynamic forces due to elastic deformations $[GF_A(t)]$ can be written in the Laplace domain as

$$\{GF_A(s)\} = -q[Q(s)]\{\xi(s)\} \quad (11)$$

where $[Q(s)]$ is the aerodynamic force coefficient (AFC) matrix. AFC matrices are typically available as a function of the reduced frequency $[Q(ik)]$. These are used via rational function approximation to generate a state-space aerodynamic model in the form

$$[Q(p)] = [A_0] + [A_1]p + [A_2]p^2 + [D]([I]p - [R])^{-1}[E]p \quad (12)$$

where p is the nondimensional complex Laplace variable $p = (sb/V)$. Substitution yields

$$[Q(s)] = [A_0] + \frac{b}{V}[A_1]s + \frac{b^2}{V^2}[A_2]s^2 + [D]\left([I]s - \frac{V}{b}[R]\right)^{-1}[E]s \quad (13)$$

With the formulation of the AFC of Eq. (13), the aeroelastic equation of motion can be written as

$$\dot{x}_{\text{AE}}(t) = \bar{A}_{\text{AE}} x_{\text{AE}}(t) + \bar{B}_{\text{AEG}} GF_G(t) \qquad \xi(t) = \bar{C}_{\text{AE}} x_{\text{AE}}(t) \quad (14)$$

where the new state vector is

$$\{x_{\text{AE}}(t)\} = \begin{Bmatrix} \xi \\ \dot{\xi} \\ x_A \end{Bmatrix} \quad (15)$$

and where $\{x_A\}$ is the augmented aerodynamic state vector,

$$\{x_A(s)\} = \left([I]s - \frac{V}{b}[R]\right)^{-1}[E]\{\xi(s)\} \quad (16)$$

and

$$\bar{A}_{\text{AE}} = \begin{bmatrix} 0 & I & 0 \\ -\bar{M}^{-1}[GK + qA_0] & -\bar{M}^{-1}\frac{qb}{V}A_1 & -q\bar{M}^{-1}D \\ 0 & E & \frac{V}{b}R \end{bmatrix}$$
$$\bar{B}_{\text{AEG}} = \begin{bmatrix} 0 \\ \bar{M}^{-1} \\ 0 \end{bmatrix} \qquad \bar{C}_{\text{AE}} = [I \quad 0 \quad 0] \qquad \bar{M} = GM + \frac{qb^2}{V^2}A_2 \quad (17)$$

Since the gust excitation forces from CFD analysis are provided in discrete time, the state-space aeroelastic equation of motion is also formulated in discrete time, as

$$\begin{aligned} x_{\text{AE}}(n+1) &= A_{\text{AE}} x_{\text{AE}}(n) + B_{\text{AEG}} GF_G(n) \\ \xi(n) &= C_{\text{AE}} x_{\text{AE}}(n) \end{aligned} \quad (18)$$

where

$$A_{\text{AE}} = e^{\bar{A}_{\text{AE}}T} \qquad B_{SG} = \int_0^T e^{\bar{A}_{\text{AE}}\tau}\,\mathrm{d}\tau \bar{B}_{\text{AEG}} \qquad C_{\text{AE}} = \bar{C}_{\text{AE}} \quad (19)$$

Finally, introducing the convolution-based gust excitation force into Eq. (18), the discrete-time state-space aeroelastic system equation of motion in response to gust excitation is written as

$$\begin{aligned} x_{\text{AE}}(n+1) &= A_{\text{AE}} x_{\text{AE}} + B_{\text{AEG}} \sum_{k=1}^{n+1} \dot{w}_G(k) GF_{\text{SEG}}(n+1-k) \\ \xi(n) &= C_{\text{AE}} x_{\text{AE}}(n) \end{aligned} \quad (20)$$

III. Numerical Application

A. Aircraft Model

The numerical test case is that of a generic transport aircraft. The model includes a fuselage, wing, aileron, and an all-movable tail. The wing and tail are both tapered and swept aft, with no twist, incidence, or dihedral angle. The cross-sectional profiles of the wing and elevator are NACA0012 symmetric airfoils. Table 1 summarizes the wing and tail geometrical dimensions. The fuselage is 20 m long with the nose 7.3 m forward of the wing leading edge, and the aft end is 2.9 m behind the tail trailing edge. It has a circular cross section with radius of 0.8 m, which tapers near the ends. The reference chord is 2 m and the reference area is 20 m^2.

Figure 1a presents the structural finite element model of the aircraft. The wing and tail are modeled by their torsion boxes, which include skin, ribs, spars, and stringers. The fuselage is modeled as a flexible bar. MSC Nastran modal analysis provided the 13 low-frequency vibration modes, including two rigid-body modes that were used for gust analysis. The ZAERO linear panel model served

Table 1 Wing and tail geometrical properties

	Wing	Tail
Span, m	10.0	4.0
Aspect ratio	10.0	6.4
Root chord, m	3.0	1.5
Leading-edge sweep angle, deg	20.0	20.0
Taper ratio	0.333	0.667

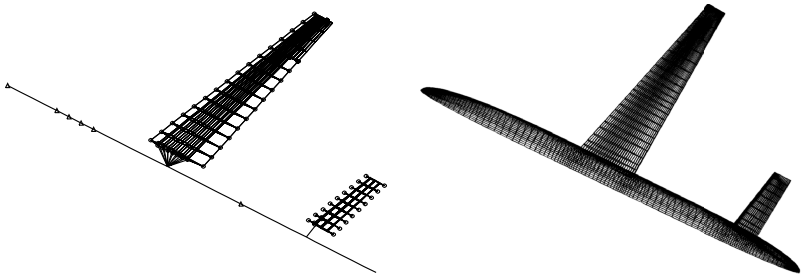

a) b)

Fig. 1 Illustrations of a) finite element model and b) CFD surface mesh of the generic transport aircraft.

for validation purposes, for comparison of CFD results with linear-aero results at the linear Mach and angle-of-attack range. The ZAERO software was also used to generate a state-space aeroelastic model of the aircraft, which served in the gust-response analysis. The linear panel aerodynamic model includes the wing, the all-movable tail, and the fuselage.

CFD analysis was performed by the EZNSS code [8]. EZNSS is a finite difference code, capable of solving the steady or time-accurate Navier–Stokes or Euler equations, using various algorithms. The current study involves mostly time-accurate Euler simulations, using the Steger–Warming solver algorithm. The aeroelastic scheme (elastic deformations and grid-update algorithm following elastic deformations) is presented in [16].

The airplane was modeled using five overlapping (chimera) grids zones. Figure 1b presents the fuselage, wing, and tail surface grids. Not shown are the two Cartesian collar zones that are used for boundary conditions transfer between the wing and fuselage and between the tail and fuselage. The total number of grid points is about 570,000. This grid is very coarse and probably not suitable for capturing the exact shock wave location and strength. However, it does capture shock wave phenomena and the associated flow nonlinearities, and provides for quick CFD analyses. All of the time-accurate CFD simulations were computed with a nondimensional time step of 0.01, which corresponds to a real time step of 3.04×10^{-5} s.

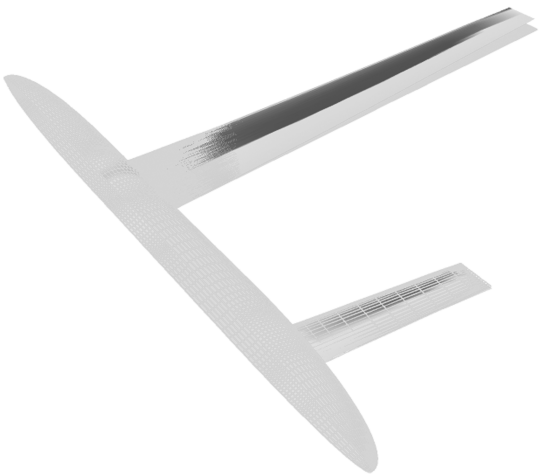

Fig. 2 Pressure distribution on the deflected configuration at 1 *g* level flight, Mach 0.85, and 10,000 ft (undeflected configuration shown in gray).

B. Trim Analysis in the Transonic Flight Regime

The elastic airplane configuration was trimmed for 1 *g* level flight at Mach 0.85 and an altitude of 10,000 ft, using the CFD-based trim analysis method of [16]. Trimmed parameters were calculated as angle of attack of $\alpha = 1.0°$ and control surface deflection angle of $\delta_e = -2.8°$ (tail deflected nose-down). Figure 2 presents the pressure distribution on the deflected configuration, at the above flight conditions, showing shock waves along the span of both the wing and tail. Also shown is the undeflected configuration, in light gray mesh, for reference. The wing is twisted nose-down, therefore reducing the load per mean angle of attack. This is due to the aft chordwise location of the center of pressure, due to the shock wave.

The discrete gust design criteria of the U.S. Federal Aviation Administration [17] requires dynamic load analysis in response to gusts of vertical velocity of 17 m/s. Flying at altitude of 10,000 ft, and Mach 0.85, a gust vertical velocity of 17 m/s induces an equivalent angle of attack of about 3.5°. Together with the trim angle of attack of 1.0°, the aircraft is subjected to an angle of attack of 4.5°. Figure 3 presents aerodynamic coefficients versus mean angle of attack at Mach 0.85 for the elastic and rigid-aircraft configurations. From Fig. 3, for an angle of attack of 4.5°, the aerodynamic forces deviate from the linear trend. The 1 *g* level-flight condition at Mach 0.85 and altitude of 10,000 ft will therefore serve as the starting conditions for the study of gust response in nonlinear flow conditions.

C. Sharp-Edge Gust Response

Figure 4 presents the time history of the lift coefficient, normalized by the steady-state lift-coefficient value, that develops in response to a sharp-edge gust excitation of equivalent angle of attack of 1° at

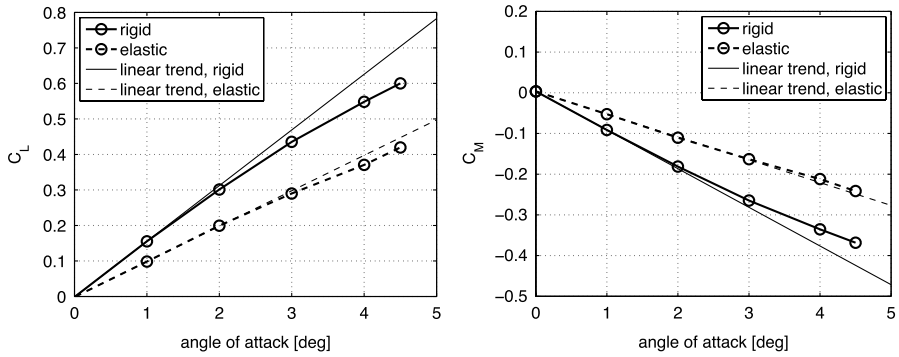

a) b)

Fig. 3 Plots of a) lift coefficient and b) moment coefficient about the center of gravity; rigid and elastic configurations; Mach 0.85, and 10,000 ft.

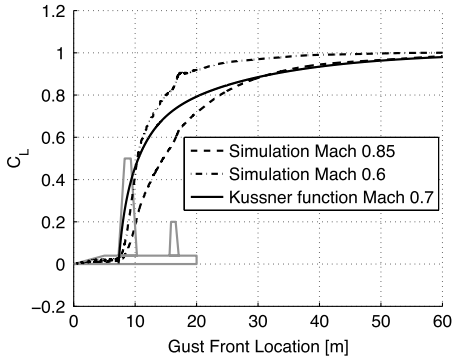

Fig. 4 Lift-coefficient time history in response to a sharp-edge gust of amplitude $\alpha_g = 1°$; Mach 0.85, 10,000 ft, $\alpha_m = 0°$, and rigid configuration.

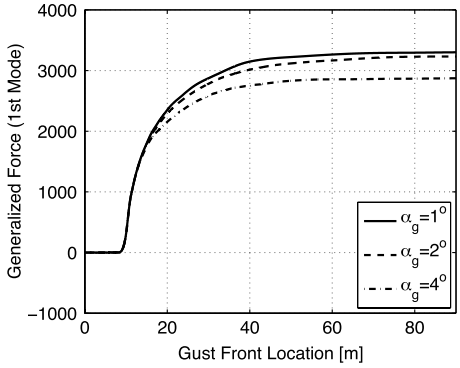

Fig. 6 Gust generalized aerodynamic forces in response to a sharp-edge gust of various amplitudes; Mach 0.85, 10,000 ft, $\alpha_m = 1°$, and rigid configuration.

flight conditions of Mach 0.85, 10,000 ft altitude, and mean angle of attack of $\alpha_m = 0°$ on the rigid-aircraft configuration. The time scale of Fig. 4 is normalized according to $s = tV/b$, where b is the semichord length. Since the semichord length is taken to be 1, the lift-coefficient history in Fig. 4 is presented as a function of the gust front location. Figure 4 shows that the aerodynamic forces due to the sharp-edge gust start to develop approximately when the gust front reaches the wing root leading edge. It also shows a slight change in the lift-coefficient value when the gust front hits the tail. For comparison, Fig. 4 also presents the closed-form Kussner function for the development of the aerodynamic forces on a flat plate at Mach 0.7 [18] and for the lift-coefficient history of a response to sharp-edge gust at Mach 0.6 [6]. All responses are normalized by their respective steady-state values. It is seen that the aerodynamic forces develop slower as Mach number is increased (a delay that is also predicted by linear theory).

Figure 5 presents the time histories of the GGAFs associated with the first three elastic modes that develop in response to a sharp-edge gust excitation of equivalent angle of attack of 1°, at flight conditions of Mach 0.85, 10,000 ft altitude, and about a mean angle of attack of $\alpha_m = 1°$. The mean angle of attack is that of trimmed conditions, as this response will be used (in convolution) to compute gust forces about trimmed flight. The GGAFs were computed at each time step of the CFD simulation by multiplying the surface forces by the modal displacements. Mode 1, with the largest generalized force, is associated with the wing's first bending. Mode 2 is an elevator (tail) mode: hence, the relatively small modal forces and the sharp increase in the response when the gust front hits the elevator. The time histories were simulated over 20,000 CFD iterations, after which the GGAFs were well converged to their final values. Sharp-edge gust responses were also computed for gust excitations of equivalent angles of attack of 2 and 4°, at the same conditions (Mach 0.85, 10,000 ft altitude, mean angle of attack of $\alpha_m = 1°$, and rigid configuration). Figure 6 presents the GGAFs in the first mode due to the various gust input angles, normalized by the input gust angle (the initial values at time zero, which correspond to the steady $\alpha_m = 1°$ flow from which the response was started, were deducted from the responses). As expected, the sharp-edge gust responses to the various input gust angles deviate from linearity as the gust amplitude is increased. Therefore, the sharp-edge amplitude to be used in the convolution should be selected according to the amplitude of the response to be computed. For example, in order to compute response to one-minus-cosine excitation of 3.5°, the sharp-edge gust response to amplitude of 4° will be used.

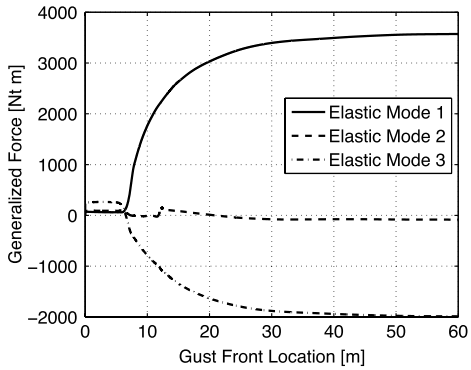

Fig. 5 Gust generalized aerodynamic forces in response to a sharp-edge gust of amplitude $\alpha_g = 1°$; Mach 0.85, 10,000 ft, $\alpha_m = 1°$, and rigid configuration.

D. Response to General Gust Input: Rigid-Aircraft Configuration

The GGAFs in response to sharp-edge gust of 4° were used in convolution, according to Eq. (5), to compute the GGAFs due to one-minus-cosine gust excitations, as defined by Eq. (6), with gradient lengths of $L_G = 25$ and 50 m, equivalent induced angle of attack of 3.5°, and mean angle of attack of $\alpha_m = 1°$ for the rigid configuration. The choice of mean angle of attack and gust intensity were such that they represent a gust as required by the Federal Aviation Regulations, on top of trimmed flight, as computed in Sec. III.B. Figure 7 presents the GGAFs that develop in response to these gust inputs as computed via convolution, compared with the GGAFs computed directly in a CFD simulation. In both cases the convolution-computed GGAFs were larger than the CFD-simulated GGAFs. In the first mode, in which the GGAFs are the largest, the errors in the convolution computation were 7.8 and 12% for the $L_G = 25$ and 50 m cases, respectively. The maximum response computed by convolution lags slightly behind the CFD-simulated maximum response. While those discrepancies are not large, it is noted that the quality of the convolution-computed response is not as good as it is for the lower Mach of 0.6 [6], in which case the differences between the convoluted and direct responses are not discernible. This is probably due to the nonlinearity of the sharp-edge gust response with respect to angle of attack at these flow conditions, which limits the accuracy of the linear convolution. To check this assumption, the one-minus-cosine gust response was repeated for gust amplitude of 1°, about a mean angle of attack of 1°. Based on the static analysis of Fig. 3, at these conditions the response should be linear and therefore well predicted by convolution. Figure 8 presents GGAFs computed by convolution, using the sharp-edge gust response of 1° amplitude, compared with GGAFs from direct CFD simulation. In this casem the maximum error in the convolution computation is less than 2%.

E. Rapid-Tuned Gust Analysis: Free Elastic Aircraft

Although the convolution presents some errors when used in the transonic speeds with moderate angles of attack, it still offers a tool for rapid estimation of responses to various gust inputs, based on a single sharp-edge gust response. This is significant for tuned gust analysis, in which the dynamic responses of the aircraft to one-minus-cosine gust profiles of various gradient lengths have to be studied. Figure 9 presents the GGAFs of the first elastic mode in response to one-minus-cosine excitations of gradient lengths of 25 to 150 m ($\alpha_g = 3.5°$, Mach 0.85, 10,000 ft, $\alpha_m = 1°$, and rigid

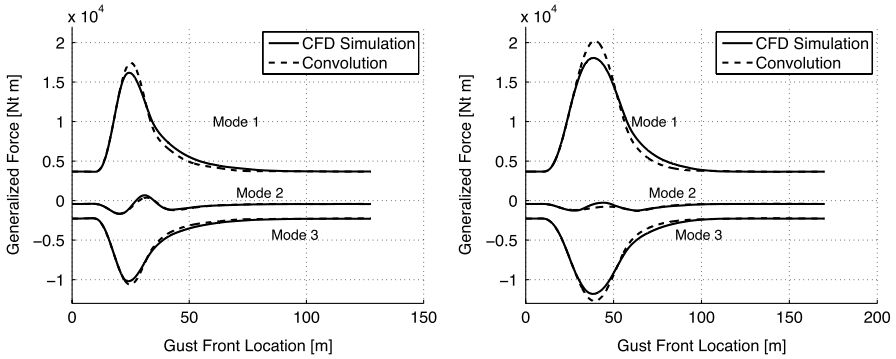

Fig. 7 Gust generalized aerodynamic forces in response to a one-minus-cosine gust of amplitude $\alpha_g = 3.5°$ and gradient length of a) 25 m and b) 50 m; Mach 0.85, 10,000 ft, $\alpha_m = 1°$, and rigid configuration.

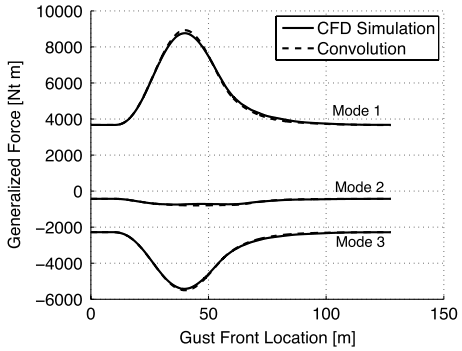

Fig. 8 Gust generalized aerodynamic forces in response to a one-minus-cosine gust of amplitude $\alpha_g = 1°$ and gradient length of 50 m; Mach 0.85, 10,000 ft, $\alpha_m = 1°$, and rigid configuration.

configuration). These responses were computed by the convolution of Eq. (5) in a few seconds. The GGAFs were then used to predict the response of the free elastic aircraft using the hybrid method presented in Sec. II.B.

A state-space discrete-time model of the aeroelastic system was created using the 13 structural modal displacements and their time derivatives as states, plus nine augmented aerodynamic lag states, totaling 35 states. The state-space aeroelastic model was created in ZAERO, based on a linear panel method, and was used to compute the tuned gust response according to Eq. (20). The state space model was computed for Mach 0.6 rather than for Mach 0.85. The reason is that the linear panel Mach 0.85 model is unstable (beyond the flutter onset) and therefore unusable. More accurate aeroelastic models could have been computed either by correcting the ZAERO model based on CFD/wind-tunnel data for Mach 0.85 and only then computing the state-space model, or by generating CFD-based reduced-order model for the aeroelastic system, as proposed in [14]. In this case the hybrid model is not expected to produce accurate gust responses. However, it is assumed that in a tuned gust analysis it will indicate which of the gust inputs results in the most critical structural response. This assumption will be verified by studying the responses to various gust gradient lengths in direct CFD simulations.

Figure 10 presents the modal displacements of the first bending mode in response to tuned gust of lengths of 25 to 150 m. The tuned gust response was computed from the hybrid model, using the Mach 0.6 linear state-space aeroelastic model and the one-minus-cosine gust forces from convolution (as presented in the previous subsection). The modal displacement in the first bending mode are representative of the intensity of the structural response, as they are correlated with wing root bending. Figure 10 shows that of the various gust lengths studied, the gust with gradient length of 50 m resulted in the largest wing bending. Therefore, this gust input will be studied in full CFD simulation of the free elastic aircraft.

Figure 11 presents modal displacements of the first wing bending as computed by a full CFD simulation. The simulation is of the free elastic airplane, in which the trimmed airplane ($\alpha = 1.0°$, $\delta_e = -2.8°$) at Mach 0.85, 10,000 ft altitude hits a one-minus-cosine gust of equivalent angle of attack of 3.5° and 50 m gradient length. A time-accurate CFD elastic simulation, which includes both the elastic modes and two rigid-body modes of heave and pitch, computes the flow parameters about the airplane as it flies past the gust. The surface pressures at each time step are used to compute the aerodynamic forces as well as the generalized forces and displacements. This simulation requires significant computational resources, but only a short time has to be simulated until the response reaches its peak. Figure 11 shows the CFD-simulated gust response versus the response from the hybrid model. It is seen that the rigid-body response is diverging. This is expected, as no pilot (control) action is taken to mitigate the effect of the gust-induced angle of attack. Again, it is noted that the hybrid model does not result in accurate estimation

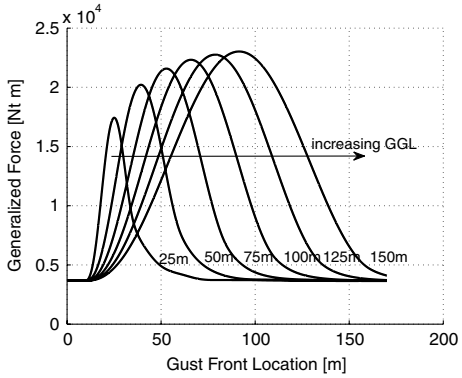

Fig. 9 Gust generalized aerodynamic force in the first elastic mode in response to a one-minus-cosine gust of amplitude $\alpha_g = 3.5°$ and various gradient lengths; Mach 0.85, 10,000 ft, $\alpha_m = 1°$, and rigid configuration.

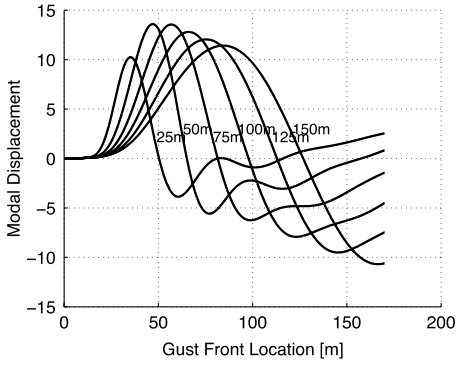

Fig. 10 Modal displacement in the first elastic mode of the free elastic aircraft in response to a one-minus-cosine gust of amplitude $\alpha_g = 3.5°$ and various gradient lengths, computed from the hybrid model; Mach 0.85, 10,000 ft, $\alpha_m = 1°$.

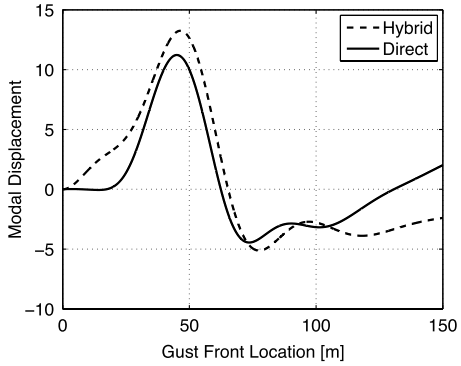

Fig. 11 Modal displacement in the first elastic mode of the free elastic aircraft in response to a one-minus-cosine gust of amplitude $\alpha_g = 3.5°$ and and gradient length of 50 m, as computed by the hybrid model and from direct CFD simulation; Mach 0.85, 10,000 ft, trimmed conditions.

of wing bending, but is only used to select the critical-gust gradient length.

To verify that the hybrid method with the Mach 0.6 aeroelastic model indeed captures the critical-gust gradient length, the responses to gusts of gradient lengths of 25 to 100 m were simulated in direct CFD analyses. Modal displacements in the first wing bending mode, Fig. 12, show that the critical response is for the 50 m gust, as predicted by the hybrid method. In general, the hybrid method could be trusted to point to the critical-gust case in cases in which the nonlinearity is mild (as is the case in this study, see Fig. 3). A small number of direct CFD simulations could be run to verify this critical case (as was done in this study). The combination of hybrid approach for pinpointing the critical-gust case (or its vicinity) and direct CFD

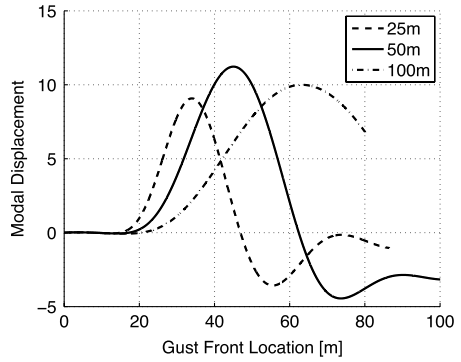

Fig. 12 Modal displacement in the first elastic mode of the free elastic aircraft in response to a one-minus-cosine gust of amplitude $\alpha_g = 3.5°$ and various gradient lengths, computed from direct CFD simulation; Mach 0.85, 10,000 ft, trimmed conditions.

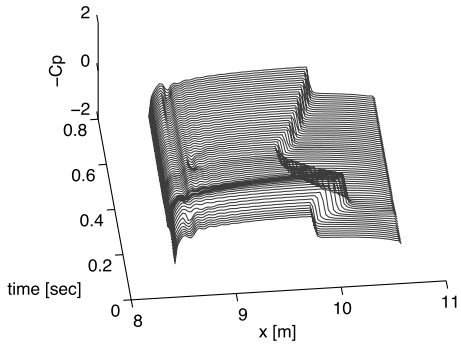

Fig. 13 Time variation of pressure coefficient along the chord in a midspan section in response to a one-minus-cosine gust of amplitude $\alpha_g = 3.5°$ and gradient length of 50 m, computed from direct CFD simulation; Mach 0.85, 10,000 ft, trimmed conditions.

simulation for analyzing the critical-gust case offers a powerful, highly computationally efficient, and accurate method for gust analysis in the transonic domain.

Figure 13 presents carpet plot of the upper surface pressure coefficient on a midspan wing section vs time, as the airplane passes the critical 50 m one-minus-cosine gust. As the gust travels along the wing chord the shock becomes stronger and is pushed downstream. The aft C_p location results in washout of the wing's outboard sections, decrease of the shock strength, and upstream motion of the shock location. This response cannot be predicted with the current practice of using linear aerodynamics for gust response. Finally, it is noted that the pressure distribution that is available from the CFD analysis at each time step during gust response can be used to compute section loads for stress analysis.

IV. Conclusions

The study presented a methodology for introducing CFD to gust-response analysis in a computationally efficient manner. Two approaches for CFD-based gust-response analysis of free elastic aircraft were presented. The direct approach involves full aeroelastic simulation within the CFD run. The hybrid approach involves computing rigid sharp-edge gust responses in a CFD run, computing the gust input forces due to arbitrary gust profiles via convolution, and applying a linear aeroelastic feedback loop to compute the aeroelastic gust responses. The latter is highly computationally efficient, as only one, relatively short CFD run is required for the computation of the sharp-edge gust response, after which responses to arbitrary gust profiles can be computed in seconds. The former is more elaborate and time-consuming, and can be used in cases of critical responses. The use of the two methods was demonstrated on a transport aircraft, flying trimmed at Mach 0.85, 10,000 ft, that passes through one-minus-cosine gust as required by the Federal Aviation Regulations. Tuned gust analysis was performed rapidly using the hybrid method, and the critical-gust response was simulated in a full CFD analysis. The study examined the validity of the use of convolution in the high transonic speeds. For the current test case, the largest errors were on the order of 10%. It is concluded that the use of convolution in the nonlinear flow regime does not yield accurate gust responses, but it can be successfully used in rapid-tuned gust analysis by the hybrid method to pinpoint the critical-gust cases, which can then be simulated by the direct CFD-based gust run.

References

[1] Karpel, M., Moulin, B., Anguita, L., Maderuelo, C., and Climent, H., "Aeroservoelastic Gust Response Analysis for the Design of Transport Aircrafts," 45th Structures, Structural Dynamics and Materials Conference, AIAA, Paper 2004-1592, Palm Springs, CA, 2004.

[2] Karpel, M., Moulin, B., and Chen, P. C., "Dynamic Response of Aeroservoelastic Systems to Gust Excitation," *Journal of Aircraft*, Vol. 42, No. 5, Sept. 2005, pp. 1264–1272. doi:10.2514/1.6678

[3] Gennaretti, M., and Mastroddi, F., "Study of Reduced-Order Models for Gust-Response Analysis of Flexible Wings," *Journal of Aircraft*, Vol. 41, No. 2, 2004, pp. 304–313. doi:10.2514/1.9325

[4] *ZAERO Theoretical Manual*, Zona Technologies, Inc., Scottsdale, AZ, Nov. 2003.

[5] Tang, D., and Dowell, E., "Experimental and Theoretical Study of Gust Response for High-Aspect-Ratio Wing," *AIAA Journal*, Vol. 40, No. 3, March 2002, pp. 419–429. doi:10.2514/2.1691

[6] Raveh, D., "CFD-Based Gust Response Analysis of Free Elastic Aircraft," *Journal of Aeroelasticity and Structural Dynamics*, Vol. 2, No. 1, 2010, pp. 23–34.

[7] Zaide, A., and Raveh, D., "Numerical Simulation and Reduced-Order Modeling of Airfoil Gust Response," *AIAA Journal*, Vol. 44, No. 8, 2006, pp. 1826–1834. doi:10.2514/1.16995

[8] Levy, Y., "Numerical Simulation of Dynamically Deforming Aircraft Configurations using Overset Grids," *Journal of Aircraft*, Vol. 38, No. 2, 2001, pp. 349–354. doi:10.2514/2.2768

[9] Parameswaran, V., and Baeder, J. D., "Indicial Aerodynamics in Compressible Flow—Direct Computational Fluid Dynamics Calculations," *Journal of Aircraft*, Vol. 34, No. 1, Jan. 1997, pp. 131–133. doi:10.2514/2.2146

[10] Singh, R., and Baeder, J. D., "Direct Calculation of Three-Dimensional Indicial Lift Response Using Computational Fluid Dynamics," *Journal of Aircraft*, Vol. 34, No. 4, July 1997, pp. 465–471. doi:10.2514/2.2214

[11] Singh, R., and Baeder, J. D., "Generalized Moving Gust Response Using CFD with Application to Airfoil-Vortex Interaction," 15th AIAA Applied Aerodynamics Conference, AIAA, Paper 1997-2208, Atlanta, 1997.

[12] Yang, G., and Obayashi, S., "Numerical Analyses of Discrete Gust Response for an Aircraft," *Journal of Aircraft*, Vol. 41, No. 6, 2004, pp. 1353–1359. doi:10.2514/1.2531

[13] Raveh, D., "CFD-Based Models of Aerodynamic Gust Response," *Journal of Aircraft*, Vol. 44, No. 3, May 2007, pp. 888–897. doi:10.2514/1.25498

[14] Raveh, D., "Identification of Computational-Fluid-Dynamics Based Unsteady Aerodynamic Models for Aeroelastic Analysis," *Journal of Aircraft*, Vol. 41, No. 3, May 2004, pp. 620–632. doi:10.2514/1.3149

[15] Karpel, M., "Design for Active Flutter Suppression and Gust Alleviation Using State-Space Aeroelastic Modeling," *Journal of Aircraft*, Vol. 19, No. 3, 1982, pp. 221–227. doi:10.2514/3.57379

[16] Raveh, D., Levy, Y., and Karpel, M., "Structural Optimization Using Computational Aerodynamics," *AIAA Journal*, Vol. 38, No. 10, 2000, pp. 1974–1982. doi:10.2514/2.853

[17] "Gust and Turbulence Loads," *Code of Federal Regulations*, Title 14, Part 25.341, Federal Aviation Administration, Jan. 2003.

[18] Bisplinghoff, R. L., Ashley, H., and Halfman, R. L., *Aeroelasticity*, Dover, Mineola, NY, 1996.